

Manuscript Type: Short Communication

MnSe₂ Nanocubes as an Anode Material for Sodium-ion Batteries

Jiasheng Qian, Shu Ping Lau

Department of Applied Physics, the Hong Kong Polytechnic University, Hong Kong SAR

Corresponding: apsplau@polyu.edu.hk

Abstract: We report a simple and scalable synthesis of MnSe₂ nanocubes as the Na-ion battery anode materials. The as-prepared MnSe₂ nanocubes electrode achieves a four-electron reaction with an enhanced reversible capacity 249 mAh·g⁻¹ at 0.1 A·g⁻¹ and a 90.8% capacity retention after 100 cycles, which could be attributed to the particle-size decreasing from micrometer to nanometer scale and the usage of diglyme-based electrolyte. This work envisions the great potential of nano-sized metal selenides toward Na⁺ ion storage.

Keywords: anode materials, sodium ion battery, MnSe₂, electrochemistry

Introduction

Sodium ion batteries (SIBs) have been of great interest due to the low cost and earth abundant of sodium resource. [1-4] In pursuit of a high performance SIB for commercial applications, recent advances have been made on the anode materials, including carbon materials, elementary substances and transition metal oxides, sulfides and selenides. [5-9] The carbon materials (i.e. graphite [10, 11] and carbon quantum dots [12]) show good cyclic stability but suffer from relatively low reversible capacities, while elementary substances (i.e. Sb [13] and P [14, 15]) and some transition metal oxides (i.e. Fe₂O₃ [16] and CuO [17]) show high theoretical capacities but suffer from poor cyclic stability. Recently, transition metal selenides, such as Cu₂Se particles, MoSe₂ microspheres and FeSe₂ microspheres, have been drawn much attention to serve as

the SIB anodes. [18-22] Particularly, the ultrasmall FeSe₂ nanoparticles were reported to show superior battery performance compared to the results of prior FeSe₂ microspheres, which could be attributed to the decreasing of particle-size from micrometer to nanometer scale. [23]

Due to the abundance, relative low cost and low toxicity, manganese-based compounds have been utilized for various energy applications. [24, 25] In particular, MnSe₂ could be a promising candidate as an electrode material due to its high theoretical capacity (503 mAh·g⁻¹). However, the potential of MnSe₂ in energy storage remains inadequately explored. [26, 27] For now, the storage behavior of nanostructured MnSe₂ toward Na⁺ ions is still unknown.

Herein, we report a one-step preparation of MnSe₂ nanocubes (MnSe₂ NCs) as an anode material for SIBs. Compared to the cyclic performance of MnSe₂ micro-particles, the as-prepared MnSe₂ NCs electrode achieves a four-electron reaction with an enhanced reversible capacity of 249 mAh·g⁻¹ at 0.1 A·g⁻¹ and a 90.8% capacity retention after 100 cycles. The electrode performance was also evaluated under carbonate-based and diglyme-based electrolytes, respectively. The results indicate a lower energy barrier of MnSe₂ NCs electrode in diglyme-based electrolyte. Our work envisions the great potential of nano-sized metal selenides toward Na⁺ ion storage.

Experimental

Synthesis of the MnSe₂ nanocubes and micro-particles: All chemicals were analytical reagents purchased from Sigma-aldrich and were used without further purification. Typically, MnSO₄ (0.338 g), Se (0.3158 g) and citric acid (3 g) were dispersed into 44 mL of distilled water. Then 16 mL of hydrazine hydrate was added into the dispersion and kept stirring for 1 h. After that, the dispersion was poured into Teflon-lined autoclave (Parr 4748) and heated up to 180 °C for 12 h. For the synthesis of MnSe₂ micro-particles, the

hydrothermal treatment needs >48 h. When the reaction was completed, the suspension was poured out for sonication and filtration. The residues were collected and dried at 80 °C in vacuum overnight.

Preparation of the MnSe₂ anode: The Cu foil was thoroughly washed by ethanol and DI water for several times. The as-prepared MnSe₂ nanocubes were well mixed with carbon black (Super P) and sodium carboxymethylcellulose (Na-CMC) in a mass ratio of 7:2:1. The mixture was coated onto the copper foil. After vacuum drying at 60 °C overnight, the MnSe₂ anode could be obtained. The mass loading of the active materials was controlled in the range of 0.8 – 1.2 mg·cm⁻² (0.9 – 1.4 mg).

Assembly of half cell: Half cells (CR2032 coin cell) were fabricated in an argon-filled Mbraun glovebox (with both H₂O and O₂ contents less than 0.5 ppm). The MnSe₂ anodes were cut into round circles with 12 mm in diameter and regarded as the working electrodes for battery test. Sodium metal was served as the counter electrode. 1.0 mol·L⁻¹ NaCF₃SO₃ dissolved in diethylene glycol dimethyl ether (diglyme) and 1.0 mol·L⁻¹ NaClO₄ dissolved in ethylene carbonate and dimethyl carbonate (EC/DMC, 50/50, v/v) were used as the electrolytes, respectively.

Materials Characterizations: Scanning electron microscopy (SEM) (Tescan MIMA3) was used to visualize the surface and cross sectional morphologies of the MnSe₂ anodes. The morphology and selected area electron diffraction (SAED) pattern of the MnSe₂ nanocubes were investigated by a JEM 2100F (field emission) scanning transmission electron microscope with an Oxford INCA x-sight EDX Si(Li) detector. XRD patterns were recorded by using a Rigaku SmartLab X-ray diffractometer operating at 45 kV and 200 mA with Cu K α source ($\lambda=1.54056 \text{ \AA}$).

Electrochemical Performance Measurements: All the electrochemical experiments were performed in ambient condition. The cyclic voltammograms (CV) and galvanostatic charge/discharge (GCD) measurements were carried out by an Arbin battery test system. The electrochemical impedance spectrum (EIS) was measured by using an electrochemical working station (CH Instrument). The galvanostatic

intermittent titration technique (GITT) plots were measured at a current density of 20 mA·g⁻¹ for 30 min followed by a resting period of 120 min. The chemical diffusion coefficient of Na⁺ ions passing through the MnSe₂ nanocubes electrode can be calculated based on the equation (1):

$$D_{\text{Na}^+} = \frac{4}{\pi} \left(\frac{mV_M}{MS} \right)^2 \left(\frac{dE_s/d\delta}{dE_\tau/d\sqrt{\tau}} \right)^2 \approx \frac{4}{\pi\tau} \left(\frac{mV_M}{MS} \right)^2 \left(\frac{\Delta E_s}{\Delta E_\tau} \right)^2 \quad (1)$$

where *m* and *M* are the mass (g) and the molecular weight (g·mol⁻¹) of MnSe₂, respectively. *S* is the effective surface area (cm²) of MnSe₂. *V_M* is the molar volume (cm³·mol⁻¹) of MnSe₂. *dE_s/dδ* is the slope of the coulometric titration curve by plotting the equilibrium electrode potential measured after each titration step *δ* (sec). *dE_τ/d√τ* is the slope of the linearized region of the potential *E_τ* during the current pulse of duration time *τ*.

Results and Discussions

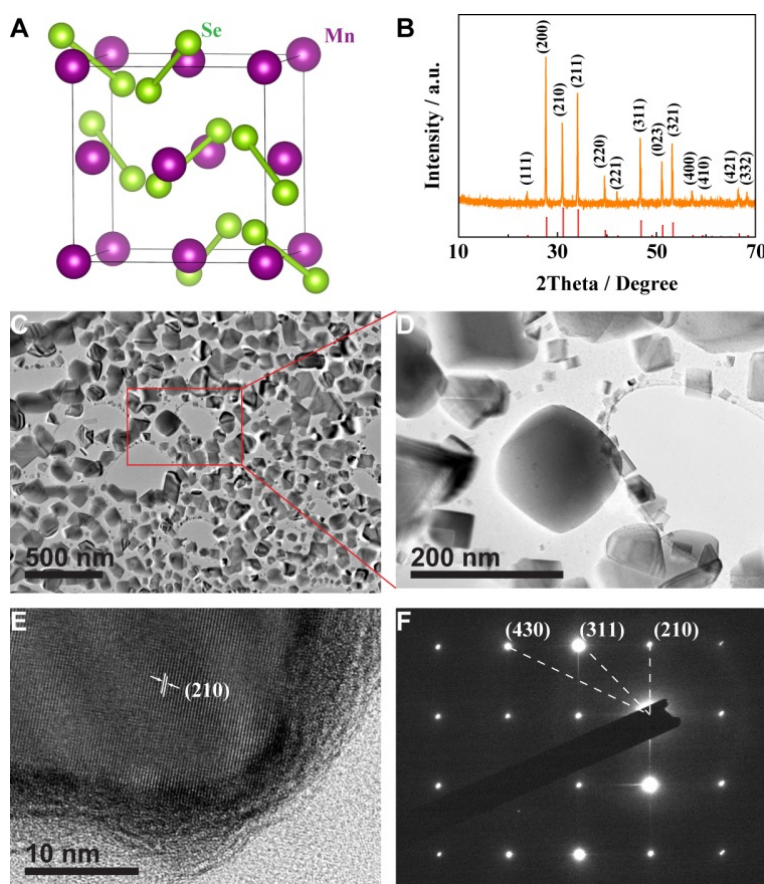
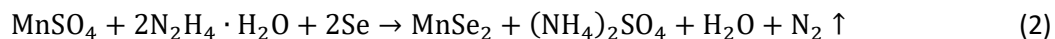


Fig. 1 Characterizations of the MnSe₂ nanocubes. A) Crystal structure. B) XRD pattern. C) low magnification TEM image. D) Zoomed-in TEM image. E) High resolution TEM image. F) SAED pattern.

The MnSe₂ NCs were synthesized *via* a hydrothermal process. The reactants including MnSO₄, Se and citric acid (CA) were dispersed into distilled water and hydrazine hydrate. During the hydrothermal treatment, the chemical reaction could be preceded as follows (2):



During the reaction process, Se is reduced by N₂H₄·H₂O to react with Mn²⁺, and the acidic CA can neutralize the excessive alkaline N₂H₄·H₂O. After hydrothermal treatment for 12 h, black MnSe₂ powder could be obtained. As shown in Fig. 1A, MnSe₂ has a cubic pyrite structure with one Mn atom on the octahedral site and six Se atoms nearby. The XRD pattern of as-prepared MnSe₂ NCs is shown in Fig. 1B, which matches well with the standard MnSe₂ phase (JCPDS card No. 73-1525). If adjusting the mass ratio of citric acid, an impurity peak belonged to Se (JCPDS card No. 86-2246) or MnSe (JCPDS card No. 11-0683) could be detected, as shown in Fig. S1 in the Supplementary Information. If the hydrothermal process is extended to >48 h, the MnSe₂ NCs will grow into micro-particles, as shown in Fig. S2. The low magnification TEM image in Fig. 1C shows large scale production (yield: ~85%) of MnSe₂ NCs with <200 nm in size. The cubic shape of the as-obtained MnSe₂ could be clearly observed from Fig. 1D. The lattice fringes assigned to the (210) reflection of MnSe₂ could be clearly seen from the high resolution TEM (HR-TEM) images in Fig. 1E and Fig. S3, demonstrating the high crystallinity of the as-prepared MnSe₂ NCs. As shown in Fig. 1F, the corresponding SAED pattern shows square diffraction dot array at d-spacings of ~2.85, 1.93 and 1.28 Å, which could be attributed to the (210), (311) and (430) reflections of MnSe₂, respectively, further confirming the yield of MnSe₂ crystals.

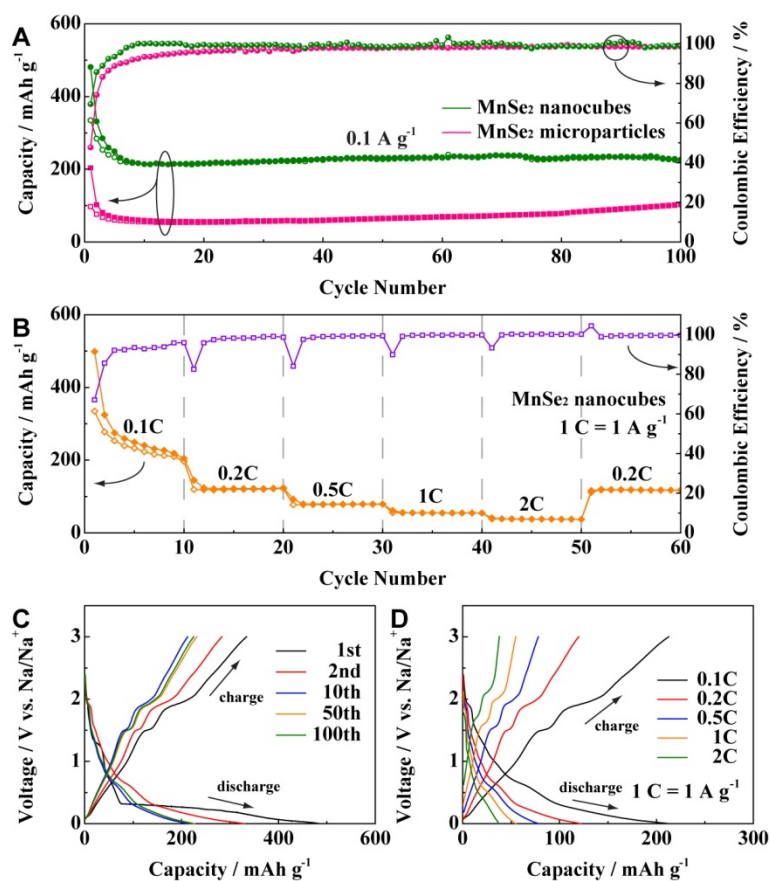


Fig. 2 Electrochemical performance investigation. A) Cyclic performance and coulombic efficiency of MnSe₂ micro-particles and nanocubes anodes at 0.1 A·g⁻¹. B) Rating capability and coulombic efficiency of MnSe₂ nanocubes anode at the current densities of 0.1 - 2 A·g⁻¹. C) GCD profiles of different cycles of MnSe₂ nanocubes anode at 0.1 A·g⁻¹. D) GCD profiles of MnSe₂ nanocubes anode at different current densities of 0.1 - 2 A·g⁻¹

To evaluate the electrochemical potential of the MnSe₂ NCs, the battery anode was fabricated by mixing MnSe₂ NCs with carbon black and binder at a mass ratio of 7:2:1. Coin cells were assembled by using MnSe₂ NCs anodes and Na metal as the working and counter electrodes with 1 mol·L⁻¹ NaCF₃SO₃/diglyme electrolyte in between. As shown in Fig. 2A, the initial capacity of the MnSe₂ NCs anode reaches 481 mAh·g⁻¹_{anode} at 0.1 A·g⁻¹, which approaches the theoretical capacity of 503 mAh·g⁻¹_{anode} (based on four-electron conversion reaction). The reversible capacity could still maintain at 249 mAh·g⁻¹_{anode} in the fifth discharge cycle and achieves a 90.8% capacity retention after 100 cycles, which could be much higher than the value of MnSe₂ micro-particles anode, even competitive with other metal selenides or graphite anodes. [10, 18-20] The cyclability enhancement is further confirmed by the EIS patterns in Fig. S4, which could be attributed to the particle-size decreasing from micrometer to nanometer scale. **Due to irreversible**

capacity loss, the MnSe₂ NCs anode shows an initial coulombic efficiency of ~70%, which could still be higher than the value of MnSe₂ micro-particles anode (48%). The coulombic efficiencies of both anodes gradually increase to ~100% after several cycles. As shown in Fig. 2B, with the increase of current densities from 0.1, 0.2, 0.5, 1 to 2 A·g⁻¹, the average capacities of MnSe₂ NCs anode (calculated based on the anode mass) remain 249, 122, 79, 55 and 38 mAh·g⁻¹_{anode}, respectively. After returning to the initial current density of 0.2 A·g⁻¹, the discharge capacity could be recovered to ca. 119 mAh·g⁻¹_{anode} when the mass loading of MnSe₂ NCs is controlled in the range of 0.8 - 1.2 mg·cm⁻². The coulombic efficiency of the MnSe₂ NCs anode still remains >98% after cyclic and rating tests, indicating a highly cyclic stability that further confirmed by the SEM images in Fig. S5. Besides, the MnSe₂ NCs anode was also tested in carbonate-based (NaClO₄/EC/DMC) electrolyte. As shown in Fig. S6, the MnSe₂ NCs anode shows an initial capacity of 475 mAh·g⁻¹_{anode} but drops dramatically to only 20 mAh·g⁻¹_{anode} after 100 cycles. Compared to the carbonate-based electrolyte, the stronger solvation ability of diglyme-based electrolyte may facilitate sodium removal from the anode upon Na⁺ ions extraction, further lowering the kinetic barrier. [1] In our case, the result that a much higher reversible capacity of MnSe₂ NCs anode is achieved in diglyme-based electrolyte rather than in carbonate-based electrolyte reveals the lower kinetic barrier of the MnSe₂ NCs anode in NaCF₃SO₃/diglyme electrolyte. The GCD profiles of MnSe₂ NCs anode in different cycles are exhibited in Fig. 2C. The irreversible capacity of the initial cycle is caused by the decomposition reaction of electrolyte and the formation of a solid electrolyte interphase (SEI). Two tiny shoulders could be observed at 2 and ~1.3 V, while a huge plateau appears at 0.3 V in first discharge cycle, confirming a typical anode-like behaviour of MnSe₂ NCs. The shoulder at ~1.3 V and the plateau at 0.3 V move to ~1.5 and 0.7 V from the second cycle, respectively. In the first charge cycle, two shoulders appear at 1.5 and 1.9 V and remain nearly unchanged in the following charge cycles. As shown in Fig. 2D, all the GCD profiles at different current densities show similar shapes, which are in accordance with the results in Fig. 2C. With the

increase of current density from 0.1 to 2 A·g⁻¹, the reversible capacity of the MnSe₂ NCs anode decreases from 249 to 38 mAh·g⁻¹_{anode}, which agrees well with the results of rating performance in Fig. 2B.

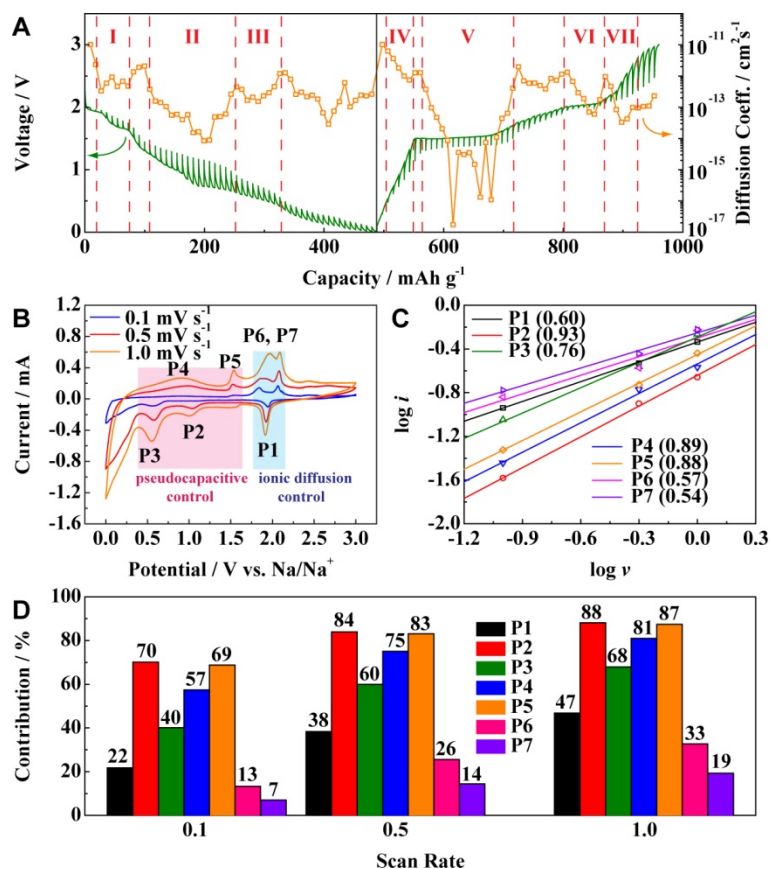


Fig. 3 Kinetics investigation. A) GITT plots of the MnSe₂ nanocubes anode at 20 mA·g⁻¹ and corresponding diffusion coefficient of Na⁺ ions. B, C) CV profiles at different scan rates and the corresponding log(*i*) versus log(*v*) plots at different redox states. D) Normalized contribution ratio of capacitive capacities at different scan rates from every redox peak of MnSe₂ NCs anode.

To investigate the kinetical characteristics of the MnSe₂ NCs anode, the GITT plots and corresponding diffusion coefficient of Na⁺ ions are shown in Fig. 3A. The shape of GITT curve could be very similar to the GCD profiles in Fig. 2C and 2D, indicating the MnSe₂ NCs anode could be close to the equilibrium during charging/discharging. [28] The corresponding Na⁺ diffusion coefficient values are mainly in the order of 10-12 cm²·s⁻¹ except for seven minimum values (three at discharge state and four at charge state), indicating that the sodiation/de-sodiation of MnSe₂ NCs anode involves multi-step conversion reactions. To further understand the electrochemical behaviors of the MnSe₂ NCs, the CV profiles at different scan rates have been shown in Fig. 3B. In accordance with the GITT results, totally seven peaks, including three anodic

peaks and four cathodic peaks, could be observed. With the increase of the scan rate from 0.1 to 1 mV·s⁻¹, the peak current increases without being proportional to the square root of the scan rate, indicating that the redox process involves both non-Faradaic and Faradaic behaviors. [29, 30] The equation related to peak current and scan rate is shown as follows (3):

$$\log(i) = b\log(v) + \log(a) \quad (3)$$

Where *i* is the peak current, *v* is the scan rate, and *a* and *b* are the adjustable parameters. If *b* = 0.5, the electrochemical reaction is controlled by ionic diffusion. If *b* = 1, the process primarily depends on pseudo-capacitive control. Fig. 3C shows the linear relationship between log(*i*) and log(*v*) plots at every redox peak. The *b* values of the seven redox peaks from P1 to P7 are 0.6, 0.93, 0.76, 0.89, 0.88, 0.57 and 0.54, respectively. Interestingly, the *b* values of three redox peaks (P1, P6 and P7) located at ~2 V are close to 0.5, while the *b* values of other four peaks (P2 – P5) are close to 1, implying that the redox behavior of MnSe₂ NCs anode is controlled by the ionic diffusion in the high potential range of 3 – 1.8 V and controlled by pseudo-capacitive characteristics in the low potential range of 1.8 – 0.4 V. Furthermore, the surface-limited capacitive (including double-layer capacitance and pseudo-capacitance) and diffusion-controlled redox contributions can be quantitatively calculated by using the following equation (4): [29]

$$i = k_1v + k_2v^{1/2} \quad (4)$$

Where *i* is the current at a given potential, *v* is the scan rate, and *k*₁ and *k*₂ are constants. The values of *k*₁ and *k*₂ can be recorded by plotting *i/v*^{1/2}~*v*^{1/2} curves, as shown in Fig. S7. Based on the *k*₁ and *k*₂ values, quantitative calculations of capacitive and redox contributions to Na storage from every redox peak of MnSe₂ NCs anode is shown in Fig. 3D. With the increase of scan rate from 0.1 to 1.0 mV·s⁻¹, the contribution ratio of pseudo-capacitive capacities from every redox peak also increases, which agrees with the results of prior reports. [31, 32] The largest ratio of capacitive contribution of every redox peak could be found at 1.0

$\text{mV}\cdot\text{s}^{-1}$, these values match well with the b values measured in Fig. 3C. The results further confirm the peaks in 3 – 1.8 V (P2 – P5) are controlled by pseudo-capacitive process while the peaks in 1.8 – 0.4 V (P1, P6 and P7) are controlled by diffusion process.

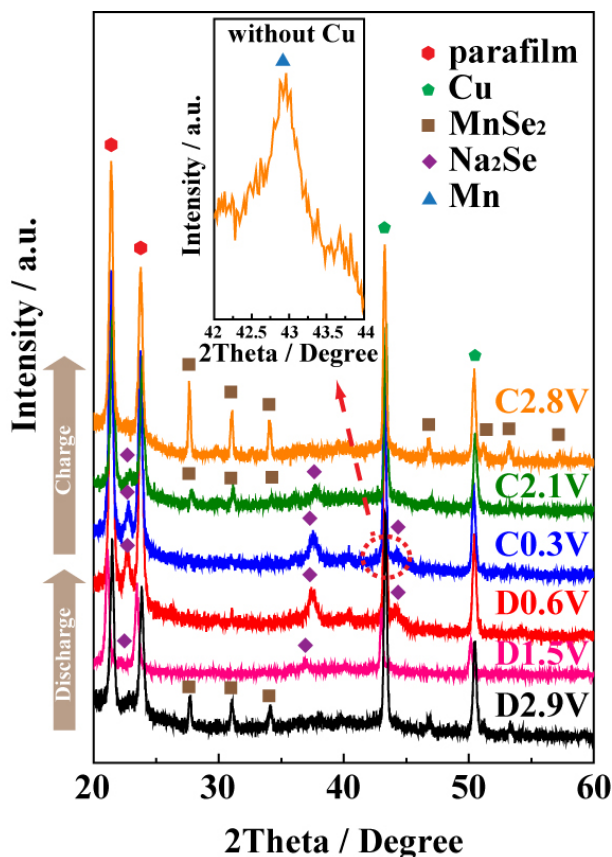
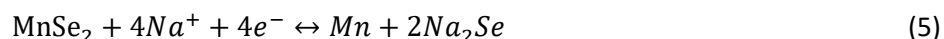


Fig. 4 Phase transformation investigation. *Ex-situ* XRD patterns at different states. (C: state of charge, D: state of discharge) Inset: *Ex-situ* XRD patterns of MnSe_2 electrode without Cu substrate at charge state of 0.3 V.

To investigate the phase transformation of the MnSe_2 NCs anode, the *ex-situ* XRD patterns at different states are shown in Fig. 4. Two sharp peaks at 21° and 24° should be attributed to the parafilm, which is used to protect the electrode from air. Another two peaks at 43° and 50° should belong to the Cu foil. When the anode discharged from 2.9 to 1.5 V, the peaks belonged to MnSe_2 disappeared. Three obvious peaks of Na_2Se (JCPDS card No. 77-2155) could be recorded at 22° , 37° and 44° when discharged to 0.6 V. However, because the characteristic peak of Mn (JCPDS card No. 17-0910) is overlapped with that of Cu at 43° , it can only be observed after removing the Cu substrate at charge state of 0.3 V, as shown in the inset figure. When charged to 2.1 V, the characteristic peaks of MnSe_2 appear again. At fully charged to 2.8 V, the

MnSe₂ peaks could be clear. The CV profiles and phase transformation analysis indicate that MnSe₂ NCs anode could achieve an overall four-electron conversion reaction as follows (5):



Conclusions

In summary, MnSe₂ NCs were successfully prepared *via* a simple and scalable hydrothermal process. The electrochemical properties of the as-prepared MnSe₂ for SIB anode have been explored. Compared to the MnSe₂ micro-particles, the MnSe₂ NCs anode achieved a four-electron reaction with an enhanced reversible discharge capacity of 249 mAh·g⁻¹ at 0.1 A·g⁻¹. After 100 cycles, a 90.8% capacity retention could be reached. Besides, the phase transformation and kinetical behavior were investigated. The Mn element and Na₂Se were found after fully discharged of MnSe₂ NCs. Details study on the phase transformation process is an ongoing project. The performance could be attributed to the nanostructured MnSe₂ and the electrolyte condition. This work envisions the great potential of nano-sized metal selenides toward Na⁺ ion storage.

Acknowledgements

This work was financially supported by Research Grants Council of Hong Kong (Project no. PolyU 153012/14P), PolyU grants (Project no. 4-BCAK and 1-ZVGH) and National Natural Science Foundation of China (NSFC, grant no. 11374250).

References

- [1] M. Lee, J. Hong, J. Lopez, Y. Sun, D. Feng, K. Lim, W. C. Chueh, M. F. Toney, Y. Cui, Z. Bao, *Nat. Energy* 2 (2017) 861-868.

- [2] Z. Hu, L. Wang, K. Zhang, J. Wang, F. Cheng, Z. Tao, J. Chen, *Angew. Chem. Int. Ed.* 53 (2014) 12794-12798.
- [3] X. Xiang, K. Zhang, J. Chen, *Adv. Mater.* 27 (2015) 5343-5364.
- [4] J. Billaud, R. J. Clément, A. R. Armstrong, J. Canales-Vázquez, P. Rozier, C. P. Grey, P. G. Bruce, *J. Am. Chem. Soc.* 136 (2014) 17243-17248.
- [5] W. Luo, F. Shen, C. Bommier, H. Zhu, X. Ji, L. Hu, *Acc. Chem. Res.* 49 (2016) 231-240.
- [6] H. Kang, Y. Liu, K. Cao, Y. Zhao, L. Jiao, Y. Wang, H. Yuan, *J. Mater. Chem. A* 3 (2015) 17899-17913.
- [7] J.-Y. Hwang, S.-T. Myung, Y.-K. Sun, *Chem. Soc. Rev.* 46 (2017) 3529-3614.
- [8] F. Xie, L. Zhang, D. Su, M. Jaroniec, S.-Z. Qiao, *Adv. Mater.* 29 (2017) 1700989.
- [9] D. Su, A. McDonagh, S.-Z. Qiao, G. Wang, *Adv. Mater.* 29 (2017) 1604007.
- [10] H. Kim, J. Hong, Y.-U. Park, J. Kim, I. Hwang, K. Kang, *Adv. Funct. Mater.* 25 (2015) 534-541.
- [11] C. Zeng, F. Xie, X. Yang, M. Jaroniec, L. Zhang, S.-Z. Qiao, *Angew. Chem. Int. Ed.* 57 (2018) 8540-8544.
- [12] H. Hou, C. E. Banks, M. Jing, Y. Zhang, X. Ji, *Adv. Mater.* 27 (2015) 7861-7866.
- [13] M. He, K. Kravchyk, M. Walter, M. V. Kovalenko, *Nano. Lett.* 14 (2014) 1255-1262.
- [14] J. Sun, H.-W. Lee, M. Pasta, H. Yuan, G. Zheng, Y. Sun, Y. Li, Y. Cui, *Nat. Nanotechnol.* 10 (2015) 980-985.
- [15] H. Hou, L. Shao, Y. Zhang, G. Zhu, J. Chen, X. Ji, *Adv. Sci.* 4 (2017) 1600243.
- [16] Z. Jian, B. Zhao, P. Liu, F. Li, M. Zheng, M. Chen, Y. Shi, H. Zhou, *Chem. Commun.* 50 (2014) 1215-1217.
- [17] L. Wang, K. Zhang, Z. Hu, W. Duan, F. Cheng, J. Chen, *Nano Res.* 7 (2014) 199-208.
- [18] K. Zhang, Z. Hu, X. Liu, Z. Tao, J. Chen, *Adv. Mater.* 27 (2015) 3305-3309.
- [19] J. Yue, Q. Sun, Z. Fu, *Chem. Commun.* 49 (2013) 5868-5870.
- [20] Y. N. Ko, S. H. Choi, S. B. Park, Y. C. Kang, *Nanoscale* 6 (2014) 10511-10515.

- [21] P. Ge, H. Hou, C. E. Banks, C. W. Foster, S. Li, Y. Zhang, J. He, C. Zhang, X. Ji, *Energy Storage Mater.* 12 (2018) 310-323.
- [22] B. Chen, H. Lu, J. Zhou, C. Ye, C. Shi, N. Zhao, S.-Z. Qiao, *Adv. Energy Mater.* 8 (2018) 1702909.
- [23] F. Zhao, S. Shen, L. Cheng, L. Ma, J. Zhou, H. Ye, N. Han, T. Wu, Y. Li, J. Lu, *Nano Lett.* 17 (2017) 4137-4142.
- [24] J. Qian, H. Jin, B. Chen, M. Lin, W. Lu, W. M. Tang, W. Xiong, L. W. H. Chen, S. P. Lau, J. Yuan, *Angew. Chem. Int. Ed.* 54 (2015) 6800-6803.
- [25] J. Qian, Y. S. Chui, G. Li, M. Lin, C. M. Luk, C. H. Mak, B. Zhang, F. Yan, S. P. Lau, *J. Mater. Chem. A* 6 (2018) 10803-10812.
- [26] Q. Peng, Y. Dong, Z. Deng, H. Kou, S. Gao, Y. Li, *J. Phys. Chem. B* 106 (2002) 9261-9265.
- [27] B. Balamuralitharan, S. N. Karthick, S. K. Balasingam, K. V. Hemalatha, S. Selvam, J. A. Raj, K. Prabakar, Y. Jun, H.-J. Kim, *Energy Technol.* 5 (2017) 1953-1962.
- [28] S. Yuan, X. Huang, D. Ma, H. Wang, F. Meng, X. Zhang, *Adv. Mater.* 26 (2014) 2273-2279.
- [29] T. Brezesinski, J. Wang, S. H. Tolbert, B. Dunn, *Nat. Mater.* 9 (2010) 146-151.
- [30] L. Yu, L. Zhang, H. Wu, X. Lou, *Angew. Chem. Int. Ed.* 53 (2014) 3711-3714.
- [31] P. Ge, H. Hou, X. Cao, S. Li, G. Zhao, T. Guo, C. Wang, X. Ji, *Adv. Sci.* 5 (2018) 1800080.
- [32] P. Ge, C. Zhang, H. Hou, B. Wu, L. Zhou, S. Li, T. Wu, J. Hu, L. Mai, X. Ji, *Nano Energy* 48 (2018) 617-629.

Supplementary Information

MnSe₂ Nanocubes as an Anode Material for Sodium-ion Batteries

*Jiasheng Qian, Shu Ping Lau**

List of Contents

Fig. S1 XRD patterns of the products prepared by using different mass of citric acid (CA).

Fig. S2 SEM images of the MnSe₂ micro-particles.

Fig. S3 Characterizations of the MnSe₂ nanocubes.

Fig. S4 EIS patterns of the MnSe₂ nanocubes and micro-particles anodes.

Fig. S5 SEM images of the MnSe₂ anodes before and after electrochemical tests.

Fig. S6 Electrochemical performance of MnSe₂ electrode in NaClO₄/EC/DMC electrolyte.

Fig. S7 Cathodic peak current dependence on the scan rate, used to determine the capacitive and redox contributions to energy storage.

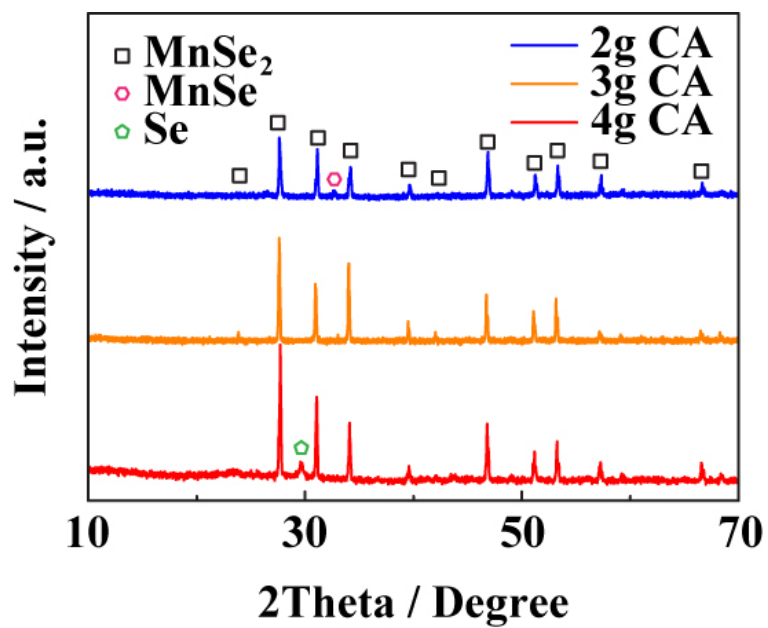


Fig. S1 XRD patterns of the products prepared by using different mass of citric acid (CA).

If less CA is added, then more Se will be reduced to react with Mn^{2+} , finally MnSe will be obtained. If excessive CA is added, then less Se will be reduced and will be the impurity in the final product.

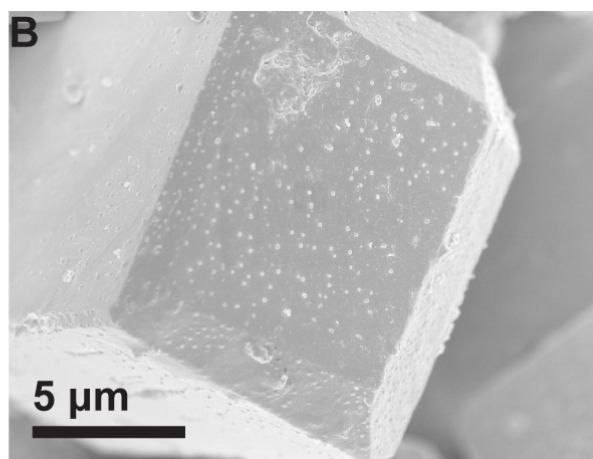
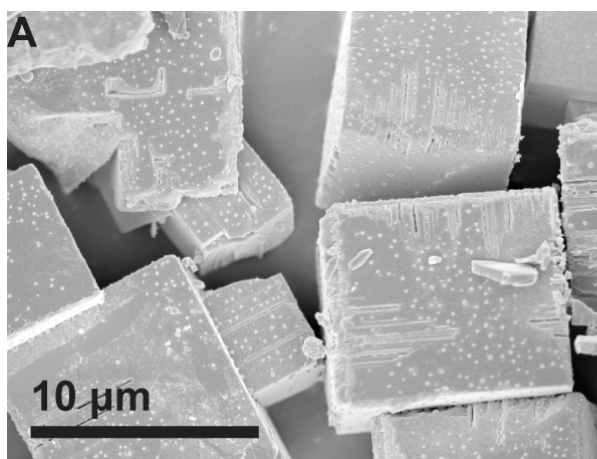


Fig. S2 SEM images of the MnSe₂ micro-particles.

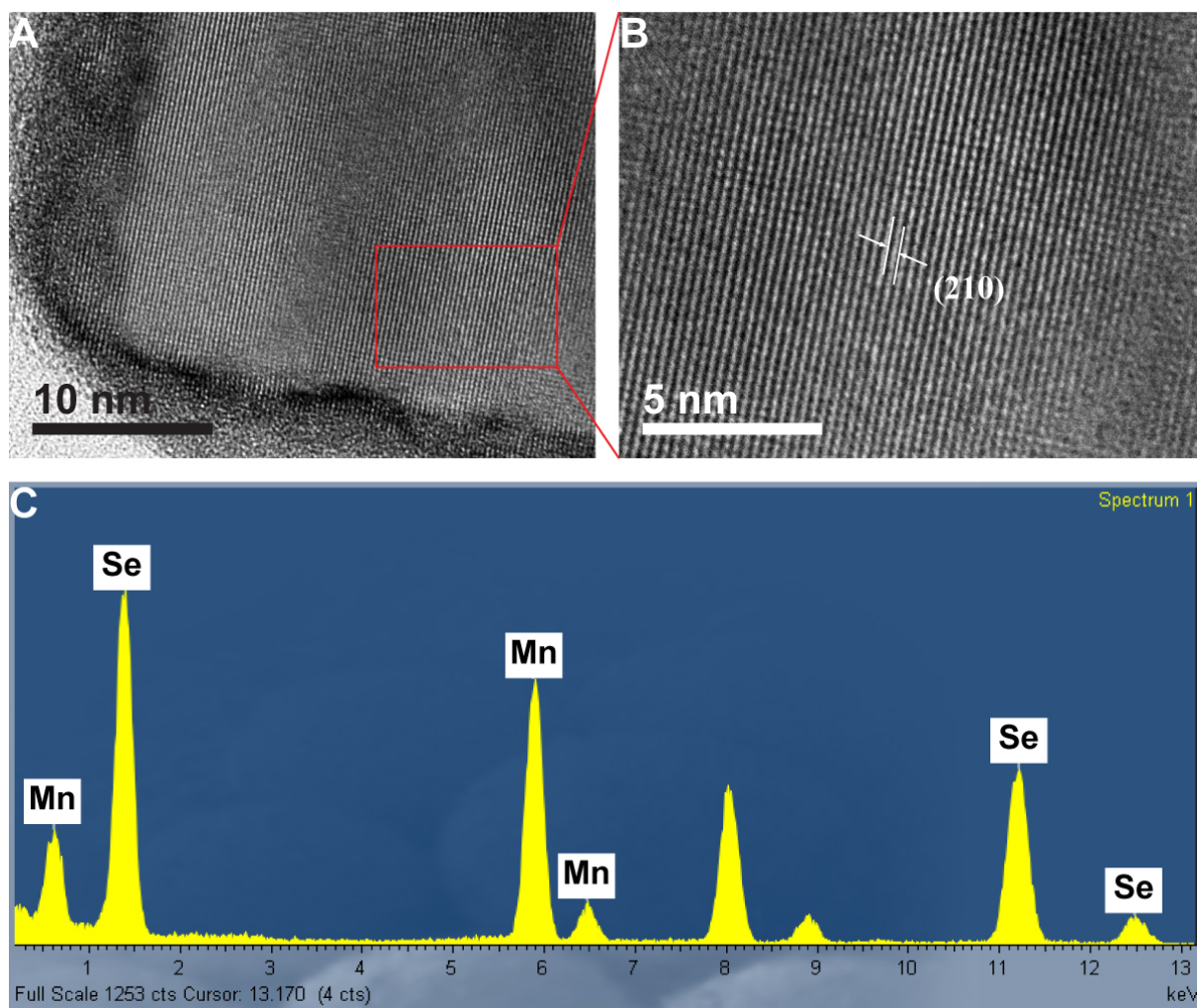


Fig. S3 Characterizations of the MnSe₂ nanocubes. A, B) High resolution TEM images. C) Corresponding EDX pattern.

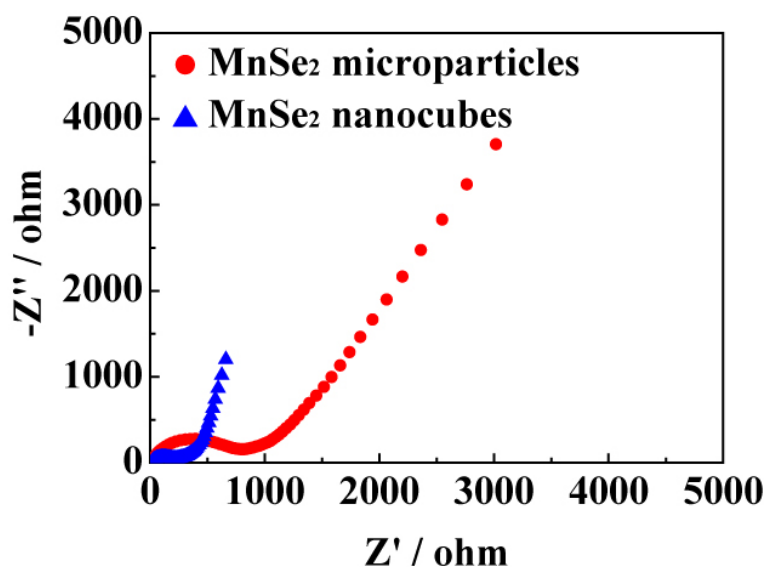


Fig. S4 EIS patterns of the MnSe₂ nanocubes and micro-particles anodes.

The EIS patterns were measured by the MnSe₂ nanocubes and micro-particles anodes after charge/discharge for five times to reach the stable states. Both the MnSe₂ nanocubes and micro-particles anodes consist of two semicircles at high and intermediate frequency region. These two semicircles are caused by the Na⁺ ions transport through the SEI layer and the interfacial charge transfer reaction combined with the electrochemical double-layer capacitive behavior, respectively. In the low-frequency region, the curve shows a straight line with an angle $\sim 45^\circ$ to the real axis, which could be attributed to the solid-state Na⁺ diffusion into the active materials. As reported previously, [S1] a larger semi-circle can be observed from the MnSe₂ micro-particles anode compared to the MnSe₂ nanocubes anode, indicating a higher resistance of the SEI formation in the MnSe₂ micro-particles anode. The result agrees well with the cyclic performance in Fig. 2A.

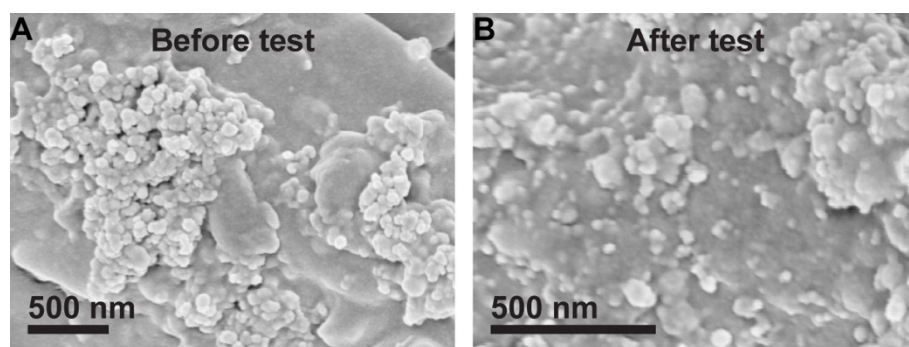


Fig. S5 SEM images of the MnSe_2 anodes before and after electrochemical tests. The SEM images show no obvious morphology change of the MnSe_2 electrodes before and after the electrochemical tests.

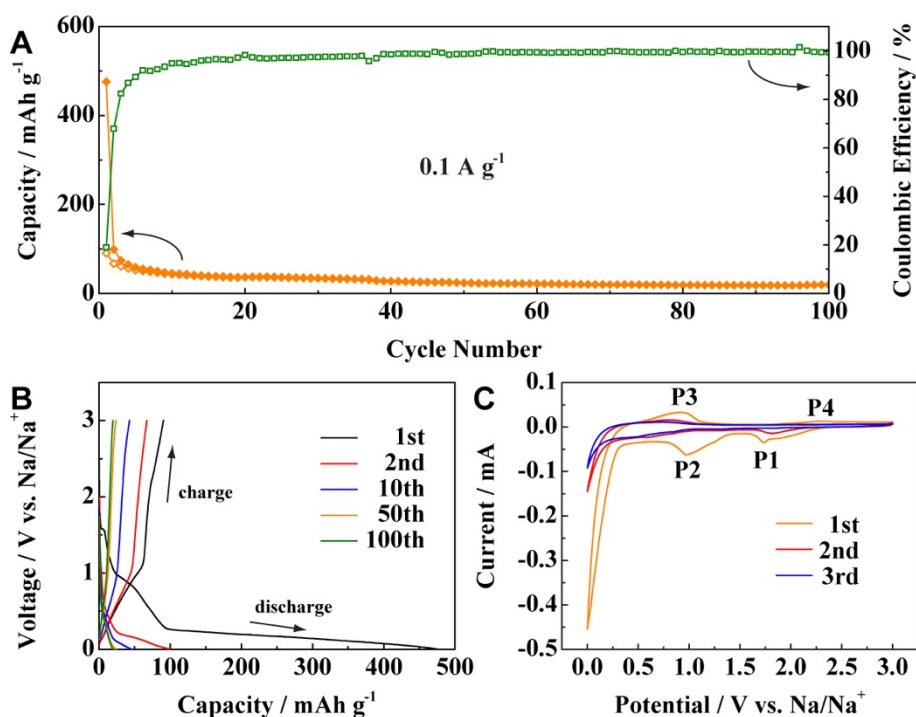


Fig. S6 Electrochemical performance of MnSe_2 electrode in $\text{NaClO}_4/\text{EC}/\text{DMC}$ electrolyte. A) Cyclic performance and and coulombic efficiency at $0.1 \text{ A}\cdot\text{g}^{-1}$. B) GCD profiles of different cycles at $0.1 \text{ A}\cdot\text{g}^{-1}$. C) CV curves of different cycles at $0.1 \text{ mV}\cdot\text{s}^{-1}$.

As shown in Fig. S5A, the initial capacity of the MnSe_2 electrode in carbonate-based electrolyte at $0.1 \text{ A}\cdot\text{g}^{-1}$ can reach $475 \text{ mAh}\cdot\text{g}^{-1}_{\text{anode}}$, but the value drops dramatically from the second cycle and remains only $20 \text{ mAh}\cdot\text{g}^{-1}_{\text{anode}}$ after 100 cycles. Despite the coulombic efficiency of the MnSe_2 electrode can reach nearly 100% except for the first several cycles, the huge irreversible capacity indicate severe side reactions involving electrolyte occurred during the SEI formation. The GCD profiles in Fig. S5B show an obvious plateau at 0.3 V in the discharge cycles, which could be similar to the GCD profile measured in diglyme-based electrolyte. Another two shoulders can be observed at 1.5 and 0.9 V only in the first discharge cycle and disappeared in the following cycles due to the capacity loss. The first charge cycle shows two shoulders at ~ 1 and 2 V , respectively, which could be attributed to the oxidation reactions to form MnSe_2 . Fig. S5C shows the CV profiles of $1^{\text{st}} - 3^{\text{rd}}$ cycles. In accordance with the results of GCD measurements, the first CV profile shows two anodic peaks at 1.7 and 1 V and two cathodic peaks at 0.9 and 2.2 V , respectively. However, the intensities of all peaks significantly reduced in the second cycle and can merely be observed in the third cycle, further demonstrating the huge capacity loss after the SEI formation in the first cycle.

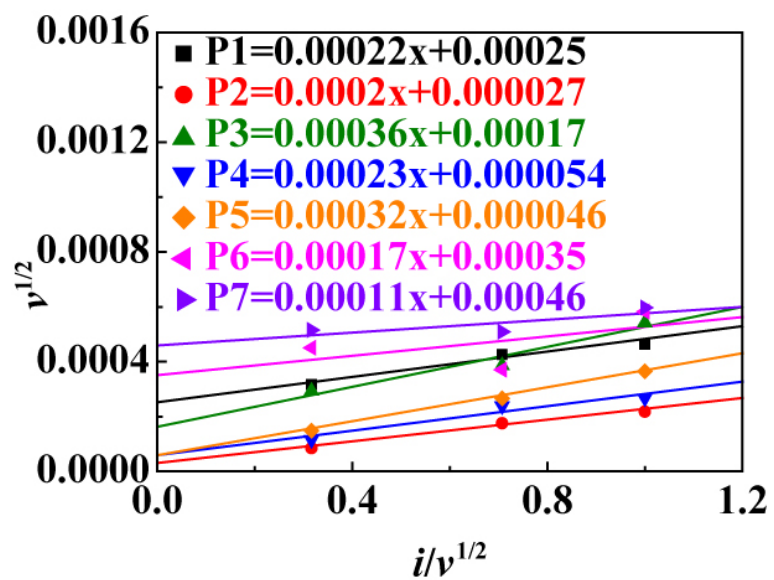


Fig. S7 Cathodic peak current dependence on the scan rate, used to determine the capacitive and redox contributions to energy storage.

References:

[S1] P. Ge, H. Hou, X. Ji, Z. Huang, S. Li, L. Huang, *Mater. Chem. Phys.* 203 (2018) 185-192.